Supplement of Atmos. Chem. Phys., 26, 2191–2208, 2026
https://doi.org/10.5194/acp-26-2191-2026-supplement

Atmospheric Chemistry and Physics
Open Access
EGU

Supplement of

Sea-to-air transfer of dissolved organic carbon via sea spray aerosol during phytoplankton bloom

Jie Hu et al.

Correspondence to: Lin Du (lindu@sdu.edu.cn)

S1. Assessing the phytoplankton bloom in the costal seawater

The Chl-a concentration data from the Copernicus Marine Data Store was checked to determine whether the collected seawater has undergone a phytoplankton bloom (https://data.marine.copernicus.eu/products). Fig. S1 below illustrates the average Chl-a concentration data for the Yellow Sea and Bohai Sea in China from May 18 to May 31, prior to our experiments (June 1 to June 18). During this period, the average Chl-a concentration at the seawater sampling location (120°33'28" E, 36°6'37" N) was 0.54 ± 0.04 mg m^{-3}, similar with our measurement of 0.43 ± 0.05 mg m^{-3} on Day 1. These concentrations are lower than that typically observed during coastal phytoplankton blooms (Delgado et al., 2023; Radoman et al., 2022). Therefore, the coastal seawater samples have not undergone a significant phytoplankton bloom prior to our experiments.

S2. Generation of nascent SSA

The main body of SSA simulation is made of transparent acrylic plastic with a volume of 180 L (length × width × height = 0.6 m × 0.5 m × 0.6 m). An overflow pipe with a slit (length × width = 20 cm × 2 mm) spans the upper space of the tank. As the centrifugal pump is running, seawater at the bottom of the tank is continuously pumped into the overflow pipe at a flow rate of 20 L min^{-1}, and after passing through the slit, a plunging waterfall is formed to hit the seawater surface to generate nascent SSA. Purified zero air (Zero Air Supply, Model 111, Thermo Scientific) enters as carrier air for the nascent SSA through the air inlet at the top of the tank and exits through the air outlet. The distance between the air inlet and the air outlet is set to 40 cm. A T-joint was set up at the air outlet to regulate fluctuations in the air flow rate between the air supply system and the sampling system. SSA sample airflow was dried by a diffusion drying tube (MD700-12F-3, Perma Pure, USA) to eliminate the effect of humidity on the SSA diameter (relative humidity <30%). All experiments were conducted at relatively constant room temperature (22–25 ℃).

S3. Assessment of damage caused by centrifugal pump operation to phytoplankton cells

During prolonged operation of centrifugal pumps, the shear forces generated can damage phytoplankton cells. To mitigate the impact of shear forces, our home-made SSA simulation tank used a parallel configuration of three centrifugal pumps. Each pump operates at its rated speed of 3500 rpm (rounds per minute), achieving a flow rate of 20 L min^{-1} and a head of 5 meters. In the nascent SSA experiments, we set the total seawater circulation flow rate at 20 L min^{-1}. Assuming each of the three parallel pumps operates at 6.7 L min^{-1} flow rate, the theoretical rotational speed for a single pump would be approximately 1167 rpm. However, given that the actual operating head is around 1.5 m, the operating speed of a single centrifugal pump should be lower than 1167 rpm. Additionally, the centrifugal pump we selected is specifically designed for low-head circulation,

with internal pressure not exceeding 0.2 bar under actual operating conditions.

Several studies have investigated the mechanical damage caused by shear forces during centrifugal pump operation to phytoplankton cells. Bronnenmeier and Märkl examined two species of green algae, *Chlamydomonas reinhardii* and *Chlorella vulgaris*, alongside the common cyanobacterium *Anacystis nidulans* (Bronnenmeier and Märkl, 1982). Their findings indicated that *Chlamydomonas reinhardii* cells exhibited critical stress thresholds of 15 to 20 bar and 2400 rpm, whereas *Chlorella vulgaris* demonstrated significantly higher thresholds of approximately 100 bar and 3000 rpm. Furthermore, *Anacystis nidulans* shows greater tolerance to shear stress than these two green algae species. During the operation of our apparatus, the rotational speed of the pump rotor and the pressure applied were significantly below the above critical values. Vandandjon et al. investigated the effects of centrifugal pump cycling on the marine diatom *Haslea ostrearia* (with an average modal length of 37.1–77.8 μm). Their results showed that cellular damage increased with higher cycling frequency, greater number of cycles, higher pump rotor speed, and larger algal size (Vandanjon et al., 1999). Specifically, when cells underwent over 1000 circulations within the pump at a circulation frequency of 0.033 s^{-1} and a rotor speed of 1320 rpm, the final cell damage rate remained around 10%. Considering that our study utilized a lower circulation frequency (0.0040 s^{-1}, completing one circulation of 84 liters of seawater within the tank at a flow rate of 20 L min^{-1} over 4.2 min), a lower number of cycles (114 to 129 cycles over 8 to 9 h), a lower rotational speed (1167 rpm), and smaller algal sizes (≤50 μm), we anticipate that the cell damage rate due to the shear effect of centrifugal pumps will be significantly lower than 10%. However, precise quantification of this damage requires further investigation.

S4. Collection of nascent SSA

A single particle sampler (DKL-2, Genstar electronic technology Co., Ltd., China) with carbon coated copper grids (T11023, Tianld Co., Ltd., China) was used to collect SSA single particles at a flow rate of 1 L min^{-1} for 30 min. The copper grids were stored in a dry environment at -20 ℃ until analyzed by transmission electron microscopy (TEM, FEI Tecnai G2 F20, Thermo Fisher Scientific, USA). After that, SSA was sampled on a low-pressure cascade impactor (DLPI+, Dekati Ltd., Finland) with a flow rate of 10 L min^{-1} for 10 h. SSA was classified into 14 stages by aerodynamic cutoff diameter within the range of 0.016-10 μm (Table S2) and collected at each stage using a quartz fiber filter (25 mm, QMA, Whatman) which was pre-baked at 550 ℃ for 6 h. These filters were divided into two fractions: a submicron sample (0.016-0.94 μm) and a supermicron sample (1.62-10 μm). Each fraction was extracted with 10 mL ultrapure water (>18.2 MΩ·cm, 25 ℃, Millipore) with ultrasound assistance for 30 min, and the extraction was filtered with 0.45 μm filter. Procedure blanks were prepared by blank quartz fiber filters with the same treatment as SSA samples. Fig. S2 shows a schematic diagram of the nascent SSA experiment.

S5. Preparation of samples and instrumental conditions for ultra-high resolution mass spectrometry

The Bond Elut PPL (Priority Pollutant) solid-phase extraction column (100 mg/3 mL, Agilent Technologies) was first activated by passing three column volumes of chromatography-grade methanol through it. Next, the packing material was rinsed with three column volumes of acidified ultrapure water (HCl = 0.01 M, pH = 2). The sample was then passed through the column at a flow rate of approximately 1 mL/min. Afterward, the packing was completely dried with high-purity nitrogen. The adsorbed organics were slowly eluted from the packing using chromatography-grade methanol. The eluate was evaporated to dryness with high-purity nitrogen and subsequently re-dissolved in a 300 μL solution (v/v = 1:1) of methanol and ultrapure water for further analysis.

Organics were separated using a C18 column (Waters, Atlantis^{TM} T3 3 μm, 2.1×150 mm). Ultrapure water (eluent A) containing 0.1% (v/v) formic acid and acetonitrile (eluent B) were used as mobile phases at a flow rate of 0.3 mL/min. The gradient elution conditions are shown in Table S4. The settings for the mass spectrometry section were as follows: source type was ESI-, capillary temperature was 275 ℃, sheath gas flow was 20 psi, aux gas flow was 5 psi, and source voltage was 4.20 kV.

S6. Parameters used to characterize the molecular formulas in the different samples

The m/z signals from the corresponding blank samples were subtracted from the aerosol and seawater samples using Xcalibur 4.2.1 software. Subsequently, MFAssignR was run in R version 4.3.2 for molecular formula assignment and data analysis. The recently developed MFAssignR is specifically designed for off-target analysis of ultra-high-resolution mass spectrometry data in complex environments and biological mixtures (Schum et al., 2020; Radoman et al., 2022). The LTQ-Orbitrap mass spectra in the m/z 150-1000 were pre-processed sequentially using the "KMDNoise" function, isotope ion filters, and internal mass recalibration before molecular formula assignment. Molecular formula assignments are limited by several conditions: signal/noise ≥ 5, $0 \le N \le 3$, $0 \le S \le 1$, $0.3 \le H/C \le 2+2/n$, $0 \le O/C \le 1$, $-10 \le DBE\text{-}O \le 10$, and error tolerance for formula assignment ≤ 3 ppm. Parameters such as double bond equivalents (DBE), aromaticity index (AI), nominal oxidation state of carbon (NOSC), and Kendrick mass defect (KMD) were used to characterize the molecular formulas in different samples.

Calculation equations of DBE (double bond equivalent), AI (aromaticity index) and NOSC (nominal oxidation state of carbon) according to the molecular elemental formula ($C_cH_hO_oN_nS_s$) assignments could be expressed as (Suo et al., 2024):

$$DBE=1+(2c-h+n)/2$$

$$AI=(1+c-o/2-h/2-s)/(c-o/2-n-s)$$

$$NOSC=4-(4c+h-3n-2o-2s)/c$$

Note that NOSC is calculated assuming that all elements are in their initial oxidation states (H = +1, O = -2, N = -3 and S = -2).

The Kendrick mass (KM) and KMD of CH2 can be directly output by MFassignR, which is calculated by the following equations:

$$KM=IUPAC\ mass\times(14/14.01565)$$

$$KMD=absolute\ (nominal\ KM-exact\ KM)$$

The intensity-weighted average values of C, H, N, O, S, m/z, O/C, H/C, AI, NOSC, DBE and KMD for each sample could be calculated by the following equation:

$$M_w=\sum(I_i\times M_i)/\sum_i I_i$$

where M represents parameters C, H, N, O, S, m/z, O/C, H/C, AI, NOSC, DBE and KMD, respectively; w notes an intensity-weighted average calculation, and I_i and M_i refer to the intensity and M value of peak i, respectively.

S7. Identification of phthalate esters in initial SML samples through mass spectrometry

Fig. S4(a) shows the base peak chromatograms for several samples: SML, seawater, submicron SSA and supermicron SSA samples on Day 1 and SML on Day 9. We observed a prominent peak (Peak 1) between elution times of 21.1 and 21.9 minutes in the SML on Day 1, significantly higher than in the seawater on Day 1 and SML on Day 9. Results in Fig. S4(b) indicate that the ion at m/z 221.0813 is the primary contributor to Peak 1, with an assigned molecular formula of $C_{12}H_{13}O_4$ (error = 1.1 ppm). The results in Fig. S4(c) show that the primary signal intensities in the secondary mass spectrometry fragments of the ion at m/z 221.0813 originate from m/z 177.0913 and 144.0964. These characteristic ions match those observed in the mass spectrum of diethyl phthalate (DEP) standard in the NIST Standard Reference Database (Fig. S4(d)). Therefore, Peak 1 can be primarily attributed to DEP. DEP is a commonly used plasticizer, and high concentrations (in the range of mg L^{-1} or mg kg^{-1}) have been detected in various aquatic environments (Gani and Kazmi, 2016; Lu et al., 2023; Liang et al., 2024). Fig. 1 reveals that high concentrations of DEP signal was present only in the Day 1 SML, while signals in the Day 1 seawater were very low. This could be due to DEP's low solubility in water and hydrophobic nature, which makes it significantly enriched in the SML. The DEP signal in the Day 9 SML was also low, likely due to reduced concentrations from biosorption or transformation processes (Gao and Chi, 2015; Liang et al., 2024). We further examined the relationship between DEP concentration and surface tension in artificial seawater (Fig. S5). Even at extremely low concentrations, DEP can significantly reduce surface tension. For example, a DEP concentration lower than 2 μM can reduce surface tension to the initial SML value of 65.84 ± 0.36 mN m^{-1}, which is significantly lower than DOC concentration in the SML at that time.

Therefore, the presence of DEP in the SML at the start of the experiment was a significant factor contributing to its low surface tension. Therefore, the presence of DEP in the SML sample at the start of the experiment was a significant factor contributing to its low surface tension.

Fig. S4a shows that DEP peaks also appeared at the same elution time in both submicron SSA and supermicron SSA samples collected on Day 1, indicating that DEP is detectable in SSA collected on that day. Due to the very low concentration of DEP compared to the total DOC concentration, the signal intensity of DEP at m/z 221.0813 accounted for 0.93% and 0.38% of the total ion current signal intensity (m/z range 150–1000) in the submicron and supermicron SSA samples on Day 1, respectively, indicating that DEP does not significantly contribute to the SSA composition. We hypothesize that this contaminant may be derived directly from the collected coastal seawater. This is supported by the following three points of evidence:

(1) Prior to the usage, the home-made SSA simulation tank was thoroughly cleaned according to the procedure described by Stokes et al. (Stokes et al., 2013). Briefly, the entire system was initially flushed with 100% isopropyl alcohol for one hour while the tank was scrubbed with a brush. This process was subsequently followed by a one-hour rinse with a 10% isopropyl alcohol and deionized water solution. Finally, the entire system was subjected to multiple rinses with deionized water, each lasting one hour. The surface tension of the deionized water reached 72 mN m^{-1} after the final rinse before we proceeded with the subsequent experiments. The aforementioned cleaning procedure ensured the removal of surface-active contaminants from the system.

(2) Based on existing literature, diethyl phthalate is employed as a plasticizer in the synthesis of polyvinyl chloride, polystyrene, and polylactic acid to improve their flexibility and plasticity (Yan et al., 2021; Paluselli et al., 2019; Mao and He, 2023; Zhao et al., 2022; Ye et al., 2020). The body of our SSA simulation tank was constructed from polymethyl methacrylate, while the pipe connections were comprised of silicone. The containers utilized to promote phytoplankton blooms were made of polycarbonate. The synthesis of these materials does not necessitate the use of phthalate plasticizers; therefore, our experimental vessels and piping cannot be considered to be direct sources of diethyl phthalate.

(3) The Shazikou Pier, from which coastal seawater is collected, serves as a significant fishing port. The surrounding waters may be adversely affected by plastic waste, fishing nets, and plastic packaging, which could potentially result in phthalate contamination (Akhbarizadeh et al., 2017; Mi et al., 2019). In fishing ports along China's Yellow and Bohai Seas, diethyl phthalate is frequently identified as the phthalate plasticizer with the highest concentration (Liu et al., 2021). Due to their high octanol-water partition coefficient and low water solubility, these compounds tend to accumulate in the sea surface microlayer relative to the bulk seawater.

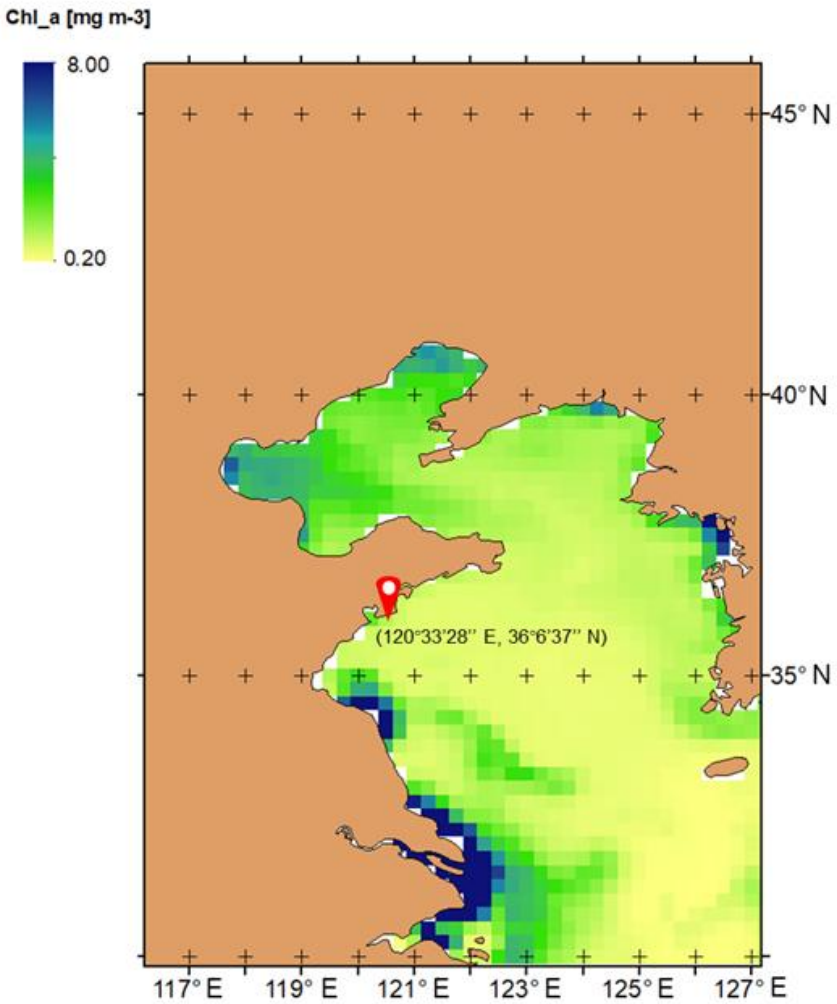

Figure S1. Coastal seawater sampling locations and the average chlorophyll-a concentration (0.54 ± 0.04 mg m^{-3}) in seawater two weeks prior to sampling.

Figure S2. Triggered the phytoplankton bloom under natural sunlight. Mesocosm experiments of phytoplankton bloom were conducted by adding 4-fold diluted Guillard's F medium in 30 transparent plastic containers.

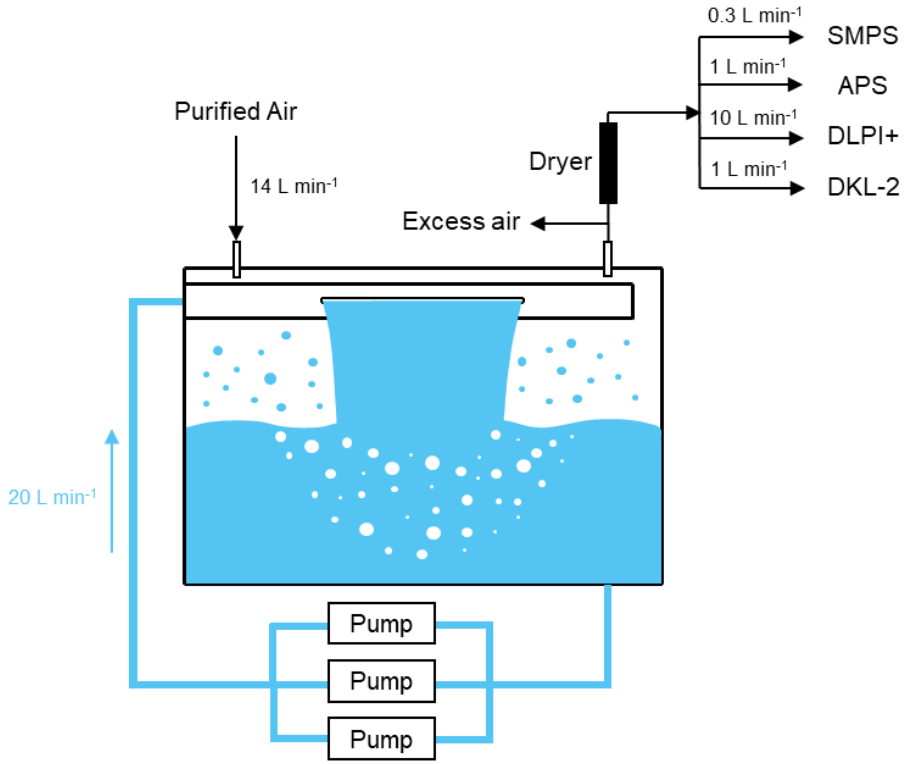

Figure S3. A schematic diagram of the nascent SSA experiment.

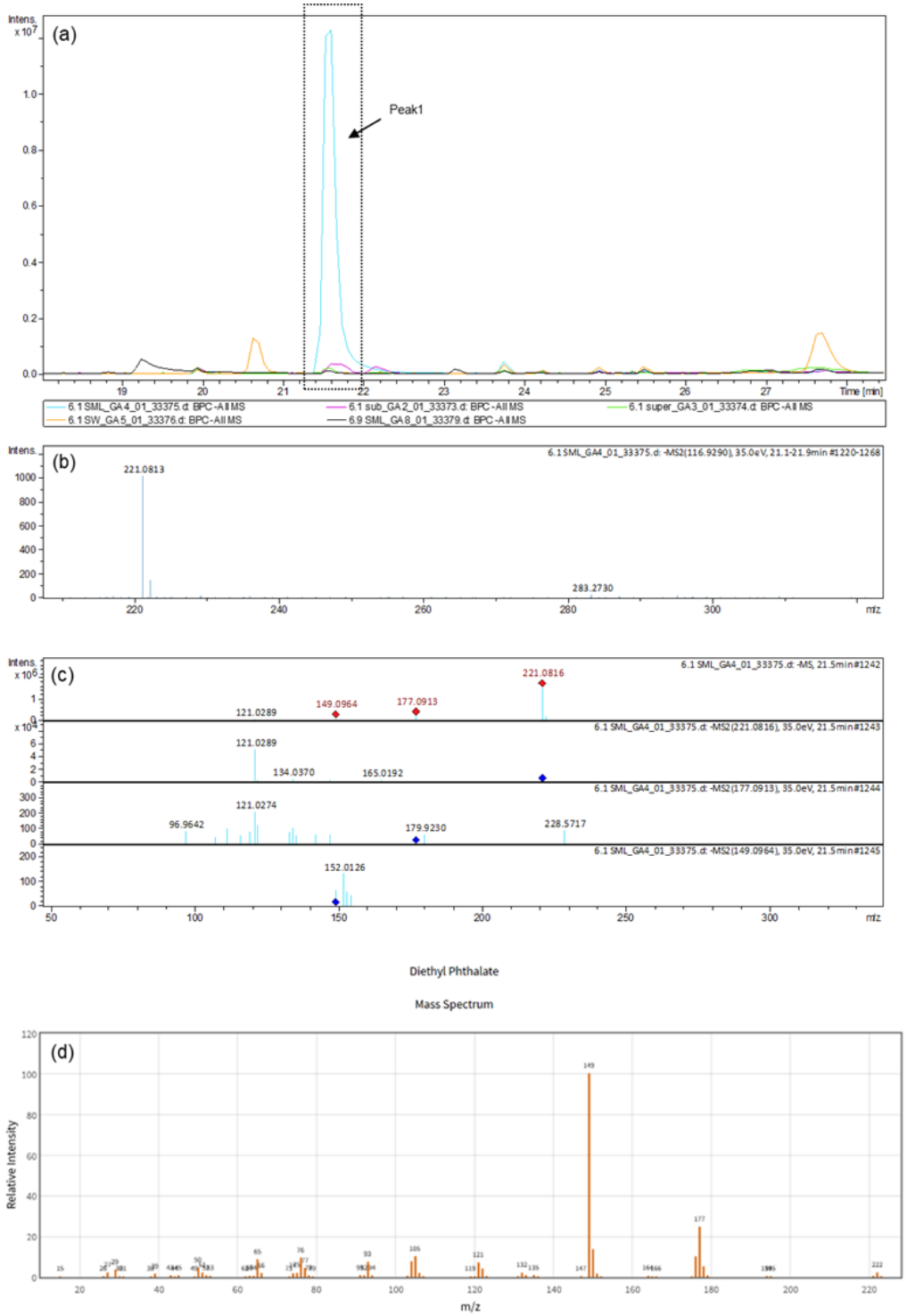

Figure S4. Identification of phthalate esters in initial SML samples through mass spectrometry. (a) Base peak chromatogram for three samples: SML sample on day 1 (blue line), seawater sample on day 1 (orange line), submicron SSA sample on Day 1 (purple line), supermicron SSA sample on Day 1 (green line), SML sample on day 9 (black line); (b) Primary contributing ion of Peak 1 and its secondary mass spectrometry fragments; (c) Standard spectrum of diethyl phthalate from NIST Standard Reference Database 69: NIST Chemistry WebBook (https://webbook.nist.gov/chemistry). Note that the standard spectrum employs electron ionization, whereas we utilize an electrospray ionization source. Nevertheless, certain characteristic ions from the standard spectrum remain useful for our identification.

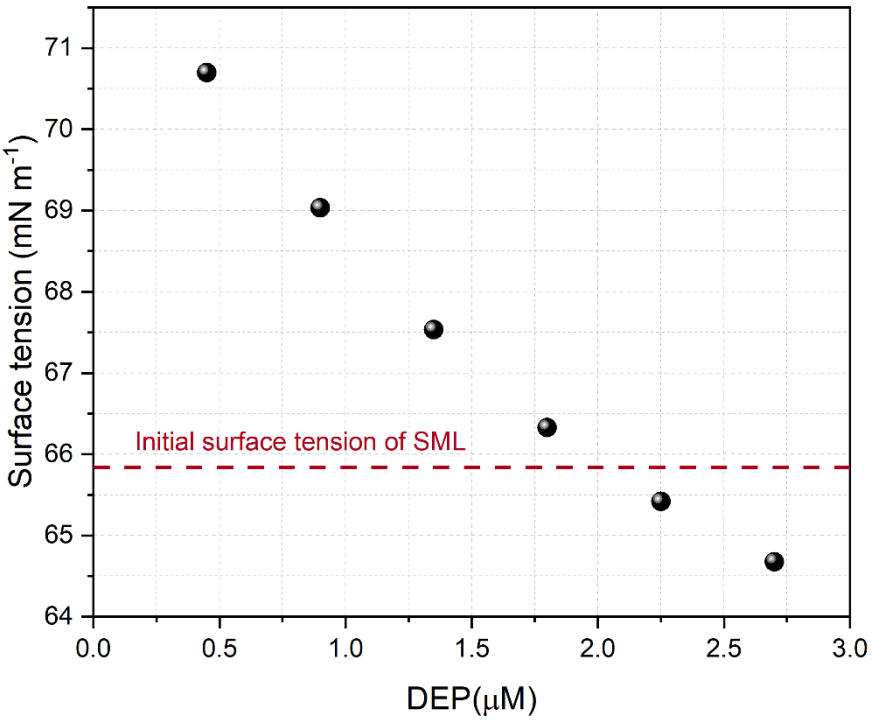

Figure S5. The relationship between different concentrations of DEP and the surface tension of artificial seawater.

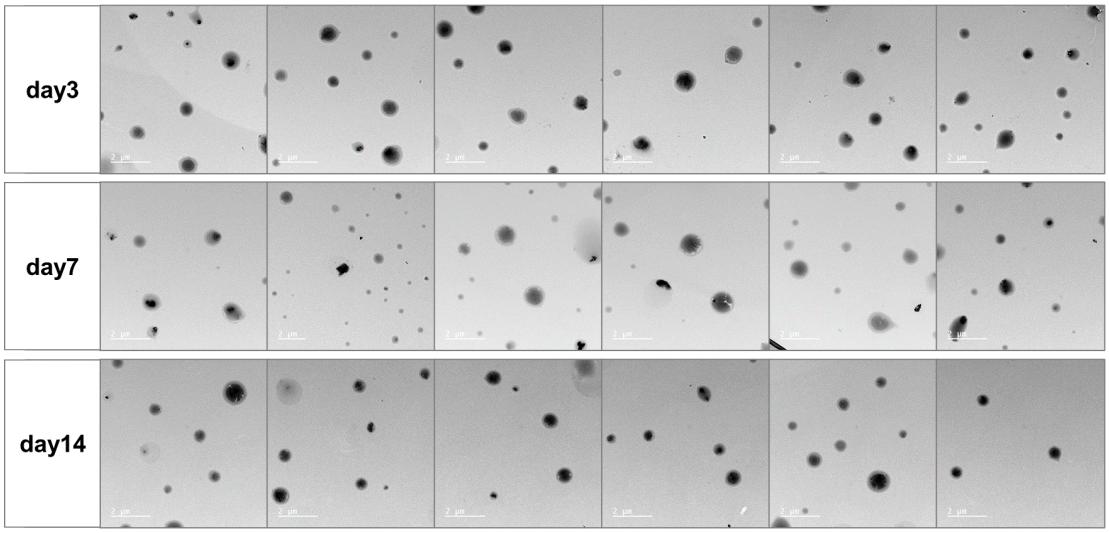

Figure S6. Transmission electron microscopy images of SSA. The sea salt core shows a black and regular shape, while the organic matter presents a gray shell encasing the sea salt core (Hu et al., 2024).

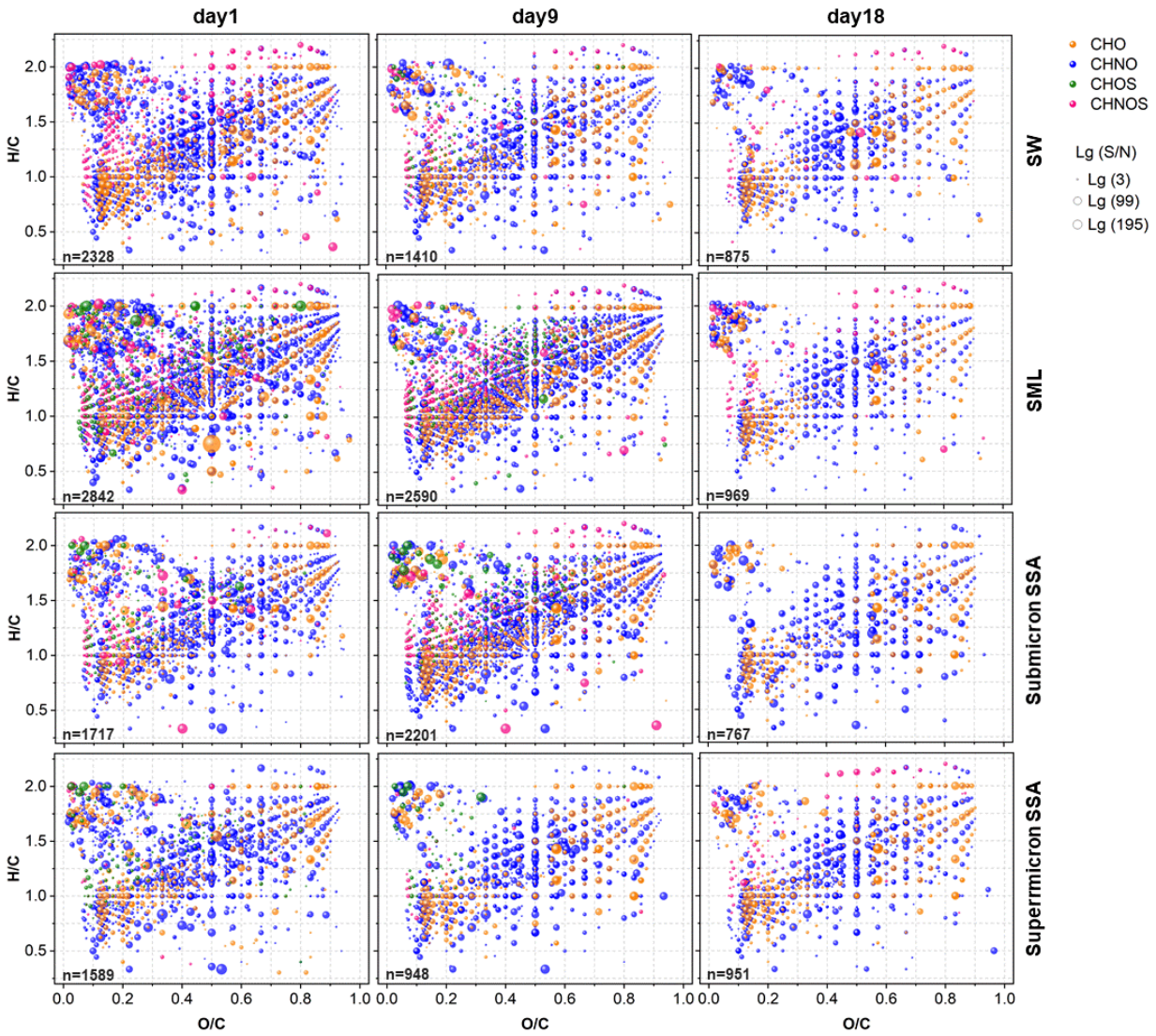

Figure S7. Sea-air transfer of organic molecules. Van Krevelen diagrams of assigned molecular formulas from different samples at the beginning, peak, and end of the phytoplankton bloom. Yellow represents CHO, blue represents CHNO, green represents CHOS, and pink represents CHNOS. To minimize the background noise in the samples, the scattered size is represented as Lg(signal/KMDnoise).

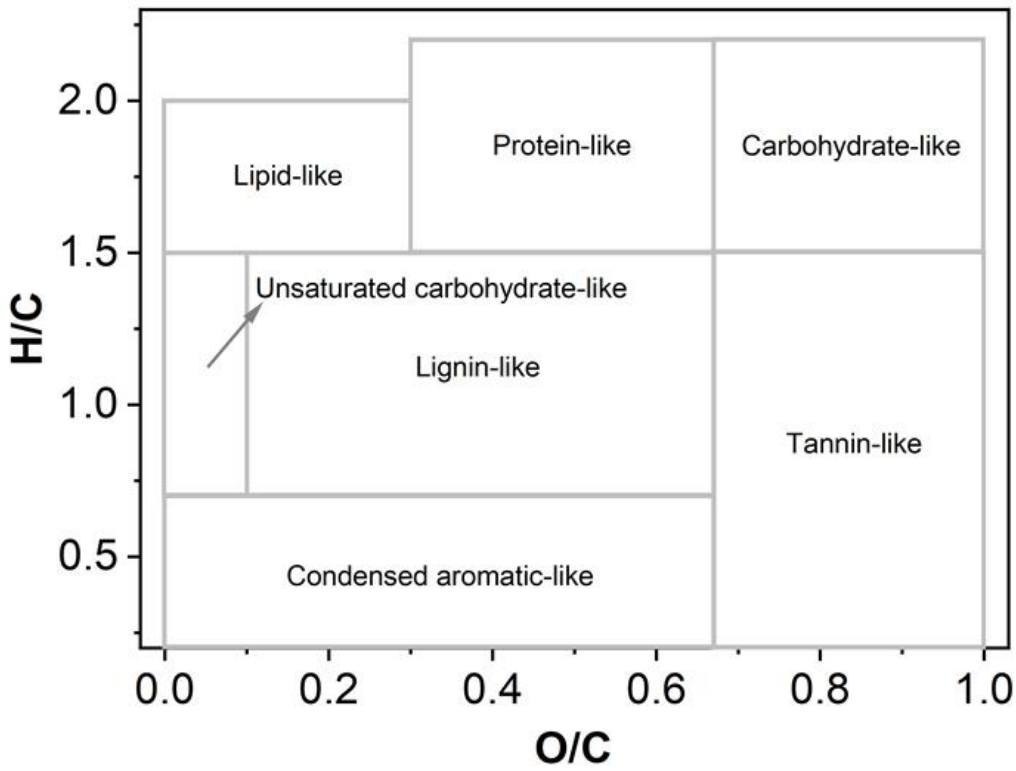

Figure S8. Chemical class regions in van Krevelen diagram space. Lipid-like ($0 < O/C \leq 0.3$; $1.5 < H/C \leq 2.0$), protein-like ($0.3 < O/C \leq 0.67$; $1.5 < H/C \leq 2.2$), carbohydrate-like ($0.67 < O/C \leq 1.2$; $1.5 < H/C \leq 2.2$), unsaturated hydrocarbon-like ($0 < O/C \leq 0.1$; $0.7 < H/C \leq 1.5$), lignin-like ($0.1 < O/C \leq 0.67$; $0.7 < H/C \leq 1.5$), tannin-like ($0.67 < O/C \leq 1.2$; $0 < H/C \leq 1.5$) and condensed aromatic-like ($0 < O/C \leq 0.67$; $0.2 < H/C \leq 0.7$) (Suo et al., 2024).

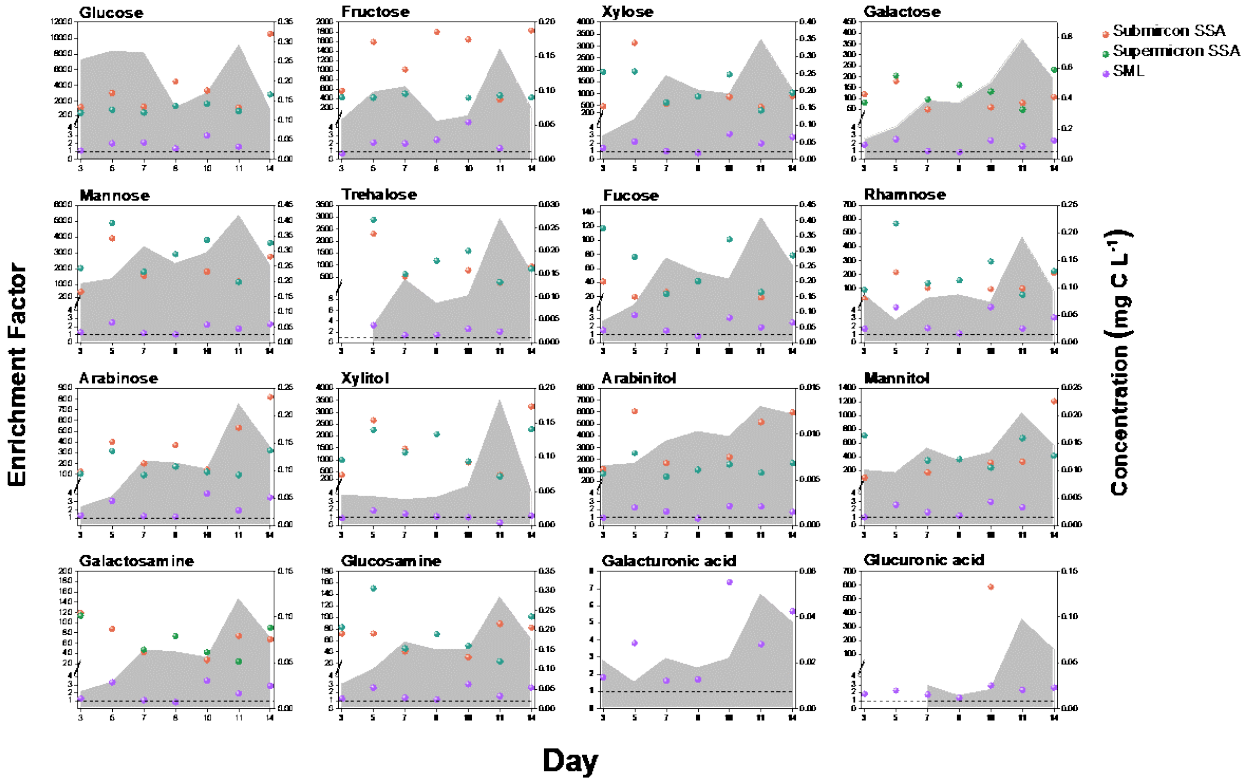

Figure S9. Fluctuations in enrichment factors of saccharides. Variation of saccharides concentration in seawater (gray shading) and their enrichment factors in SML (purple scattered points), submicron SSA (green scattered points) and supermicron SSA (orange scattered points).

Table S1. Parameter comparisons between the home-made SSA simulation tank and the Marine Aerosol Reference Tank.

Parameter	home-made SSA simulation tank	Marine Aerosol Reference Tank
Volume of Tank	180 L	210 L
Material	plexiglass	plexiglass
Material of overflow pipe	stainless steels	plexiglass
Diameter of overflow pipe	9 cm	8 cm
Internal diffuser	existence	existence
Slot size	6 mm wide × 20 cm long	6 mm wide × 20 cm long
Slot to water surface	20 cm	10 cm
Seawater circulation flow	20 L min^{-1}	15 – 70 L min^{-1}
Running mode	continuous	intermittent or continuous

Table S2. Particle size classification of the low-pressure cascade impactor.

Stage	d_{50} (μm)	Stage	d_{50} (μm)
14	10	7	0.38
13	5.34	6	0.25
12	3.63	5	0.15
11	2.46	4	0.094
10	1.62	3	0.054
9	0.94	2	0.030
8	0.60	1	0.016

Table S3. Gradient elution conditions for HPAEC-PAD(Engel and Händel, 2011).

Retention time (min)	NaOH (mM)	NaAc (mM)
0	22	0
20	22	0
21	100	0
25	100	200
35	100	200
40	75	0
45	75	0
46	22	0
55	22	0
65	22	0

Table S4. Molecular characterization of DOC in different samples at the early (D1), peak (D9), and late (D18) stages of the phytoplankton bloom.

Samples	C_w	H_w	O_w	N_w	S_w	m/z_w	DBE_w	KMD_w	O/C_w	H/C_w	AI_w	$NOSC_w$
6/01_SW	18.437	27.283	5.465	1.377	0.079	356.949	6.484	0.218	0.398	1.346	0.327	-0.162
6/01_SML	18.657	27.584	5.604	0.914	0.095	356.130	6.327	0.217	0.420	1.218	0.388	-0.159
6/01_Submicron	19.260	29.319	6.107	1.417	0.123	381.135	6.309	0.234	0.408	1.408	0.280	-0.194
6/01_Supermicron	21.424	33.675	6.186	1.421	0.050	410.472	6.297	0.231	0.386	1.422	0.305	-0.265
6/09_SW	19.884	31.710	4.526	1.328	0.068	362.728	5.693	0.185	0.368	1.412	0.305	-0.311
6/09_SML	18.514	28.560	4.846	1.468	0.134	352.282	5.968	0.201	0.386	1.400	0.297	-0.218
6/09_Submicron	19.712	30.063	5.459	1.411	0.138	377.317	6.386	0.221	0.388	1.373	0.326	-0.199
6/09_Supermicron	17.533	27.719	4.466	1.436	0.063	330.178	5.392	0.218	0.391	1.383	0.294	-0.089
6/18_SW	17.574	26.318	5.202	1.266	0.045	338.785	6.048	0.203	0.400	1.367	0.295	-0.218
6/18_SML	20.67	30.905	4.239	1.314	0.057	368.231	5.875	0.180	0.347	1.381	0.273	-0.398
6/18_Submicron	17.256	27.130	4.081	1.461	0.099	319.133	5.421	0.168	0.397	1.361	0.386	-0.126
6/18_Supermicron	14.395	21.088	4.241	1.351	0.033	280.799	5.526	0.174	0.411	1.348	0.355	-0.079

References

Akhbarizadeh, R., Moore, F., Keshavarzi, B., and Moeinpour, A.: Microplastics and potentially toxic elements in coastal sediments of Iran's main oil terminal (Khark Island), Environ. Pollut., 220, 720-731, 10.1016/j.envpol.2016.10.038, 2017.

Bronnenmeier, R. and Märkl, H.: Hydrodynamic stress capacity of microorganisms, Biotechnol. Bioeng., 24, 553-578, https://doi.org/10.1002/bit.260240304, 1982.

Delgado, A. L., Hernández-Carrasco, I., Combes, V., Font-Muñoz, J., Pratolongo, P. D., and Basterretxea, G.: Patterns and Trends in Chlorophyll-a Concentration and Phytoplankton Phenology in the Biogeographical Regions of Southwestern Atlantic, J. Geophys. Res. Oceans, 128, e2023JC019865, https://doi.org/10.1029/2023JC019865, 2023.

Engel, A. and Händel, N.: A novel protocol for determining the concentration and composition of sugars in particulate and in high molecular weight dissolved organic matter (HMW-DOM) in seawater, Mar. Chem., 127, 180-191, https://doi.org/10.1016/j.marchem.2011.09.004, 2011.

Gani, K. M. and Kazmi, A. A.: Phthalate contamination in aquatic environment: A critical review of the process factors that influence their removal in conventional and advanced wastewater treatment, Critical Reviews in Environmental Science and Technology, 46, 1402-1439, https://doi.org/10.1080/10643389.2016.1245552, 2016.

Gao, J. and Chi, J.: Biodegradation of phthalate acid esters by different marine microalgal species, Mar. Pollut. Bull., 99, 70-75, https://doi.org/10.1016/j.marpolbul.2015.07.061, 2015.

Hu, J., Li, J., Tsona Tchinda, N., Song, Y., Xu, M., Li, K., and Du, L.: Underestimated role of sea surface temperature in sea spray aerosol formation and climate effects, npj Clim. Atmos. Sci., 7, 273, https://doi.org/10.1038/s41612-024-00823-x, 2024.

Liang, J., Ji, X., Feng, X., Su, P., Xu, W., Zhang, Q., Ren, Z., Li, Y., Zhu, Q., Qu, G., and Liu, R.: Phthalate acid esters: A review of aquatic environmental occurrence and their interactions with plants, J. Hazard. Mater., 470, 134187, https://doi.org/10.1016/j.jhazmat.2024.134187, 2024.

Liu, B. X., Jiang, T., Li, Z. Y., Ge, W., Wu, J., Song, N. N., and Chai, C.: Phthalate esters in surface sediments from fishing ports in Circum-Bohai-Sea region, China, Mar. Pollut. Bull., 171,
112782, 10.1016/j.marpolbul.2021.112782, 2021.

Lu, M., Jones, S., McKinney, M., Kandow, A., Donahoe, R., Cobb Faulk, B., Chen, S., and Lu, Y.: Assessment of phthalic acid esters plasticizers in sediments of coastal Alabama, USA: Occurrence, source, and ecological risk, Sci. Total Environ., 897, 165345, https://doi.org/10.1016/j.scitotenv.2023.165345, 2023.

Mao, S. and He, C.: Effect of particle size and environmental conditions on the release of di(2-ethylhexyl) phthalate from microplastics, Chemosphere, 345, 140474-140474, 10.1016/j.chemosphere.2023.140474, 2023.

Mi, L. J., Xie, Z. Y., Zhao, Z., Zhong, M. Y., Mi, W. Y., Ebinghaus, R., and Tang, J. H.: Occurrence and spatial distribution of phthalate esters in sediments of the Bohai and Yellow seas, Sci. Total Environ., 653, 792-800, 10.1016/j.scitotenv.2018.10.438, 2019.

Paluselli, A., Fauvelle, V., Galgani, F., and Sempéré, R.: Phthalate Release from Plastic Fragments and Degradation in Seawater, Environ. Sci. Technol., 53, 166-175, 10.1021/acs.est.8b05083, 2019.

Radoman, N., Christiansen, S., Johansson, J. H., Hawkes, J. A., Bilde, M., Cousins, I. T., and Salter, M. E.: Probing the impact of a phytoplankton bloom on the chemistry of nascent sea spray aerosol using high-resolution mass spectrometry, Environ. Sci.: Atmos., 2, 1152-1169, https://doi.org/10.1039/D2EA00028H, 2022.

Schum, S. K., Brown, L. E., and Mazzoleni, L. R.: MFAssignR: Molecular formula assignment software for ultrahigh resolution mass spectrometry analysis of environmental complex mixtures, Environ. Res., 191, 110114, https://doi.org/10.1016/j.envres.2020.110114, 2020.

Stokes, M. D., Deane, G. B., Prather, K., Bertram, T. H., Ruppel, M. J., Ryder, O. S., Brady, J. M., and Zhao, D.: A Marine Aerosol Reference Tank system as a breaking wave analogue for the production of foam and sea-spray aerosols, Atmos. Meas. Tech., 6, 1085-1094, https://doi.org/10.5194/amt-7-3667-2014, 2013.

Suo, C., Zhao, W., Liu, S., Ren, Y., Zhang, Y., Qiu, Y., and Wu, F.: Molecular insight into algae-derived dissolved organic matters via Fourier-transform ion cyclotron resonance mass spectrometry: Effects of pretreatment methods and electrospray ionization modes, J. Hazard. Mater., 480, 136220, https://doi.org/10.1016/j.jhazmat.2024.136220, 2024.

Vandanjon, L., Rossignol, N., Jaouen, P., Robert, J. M., and Quéméneur, F.: Effects of shear on two

microalgae species. Contribution of pumps and valves in tangential flow filtration systems, Biotechnol. Bioeng., 63, 1-9, https://doi.org/10.1002/(SICI)1097-0290(19990405)63:1<1::AID-BIT1>3.0.CO;2-K, 1999.

Yan, Y. Y., Zhu, F. X., Zhu, C. Y., Chen, Z. H., Liu, S. C., Wang, C., and Gu, C.: Dibutyl phthalate release from polyvinyl chloride microplastics: Influence of plastic properties and environmental factors, Water Res., 204, 117597, 10.1016/j.watres.2021.117597, 2021.

Ye, X. Y., Wang, P. Y., Wu, Y. C., Zhou, Y., Sheng, Y. F., and Lao, K. J.: Microplastic acts as a vector for contaminants: the release behavior of dibutyl phthalate from polyvinyl chloride pipe fragments in water phase, Environmental Science and Pollution Research, 27, 42082-42091, 10.1007/s11356-020-10136-0, 2020.

Zhao, E., Xu, Z. N., Xiong, X., Hu, H. J., and Wu, C. X.: The impact of particle size and photoaging on the leaching of phthalates from plastic waste, Journal of Cleaner Production, 367, 133109, 10.1016/j.jclepro.2022.133109, 2022.